Journal of Physics:
Conference Series

PAPER • **OPEN ACCESS**

Design and testing of an innovative electro-dynamic filter for gas turbine intake systems

To cite this article: Michele Pinelli *et al* 2024 *J. Phys.: Conf. Ser.* **2893** 012129

Journal of Physics: Conference Series **2893** (2024) 012129 doi:10.1088/1742-6596/2893/1/012129

Design and testing of an innovative electro-dynamic filter for gas turbine intake systems

Michele Pinelli[1], Mattia Piovan[1], Alessio Suman[1]*, Nicola Zanini[1], Stefano Minotti[2], Stefano Rossin[2]

[1]University of Ferrara - Department of Engineering, Ferrara, Italy
[2]Baker Hughes, Florence, Italy

E-mail: *alessio.suman@unife.it

Abstract. Gas turbines require filtered air to preserve the efficiency and the life of the system. Different degradation processes can occur depending on the size and composition of the contaminants. The compressor's performance can be negatively impacted by fouling and erosion, which alter the shape and roughness of the blades. To limit the effects of the aforementioned phenomena, multistage filtration systems are commonly installed to reduce the contamination at the gas turbine inlet. Traditionally, particle separation is performed through mechanical filtration, which means that the particles are trapped inside cartridges of porous materials. This typology of filter guarantees a high filtration efficiency but on the other hand, generates remarkable pressure drop increasing over time. Inertial filters instead separate contaminants from the flow by utilizing the effect of inertial force acting on solid particles. In recent years, electrostatic filters have become widespread. The fibers of the filters are charged with an electrostatic field before installation and this charge is capable of separating and attracting metallic particles from the airflow. However, the electrostatic field's effect diminishes with the exposure time with this type of filter. This work presents an innovative electro-dynamic filtration system for gas turbine application. The geometry and electrical features of the devices are designed to keep low-pressure drop and high capturing efficiency over time. To achieve these goals, a numerical campaign is performed using an in-house OpenFOAM solver, which takes into account the effect of the electrostatic force of the Lagrangian phase. After the definition of the optimal geometry, experimental tests are performed to validate the numerical results. Finally, a comprehensive laboratory-scale campaign is carried out to evaluate filtration efficiency under various environmental conditions, including different types of contaminants, concentrations, and exposure times.

1. Introduction

One of the most critical components in a gas turbine is the intake filter since it preserves the efficiency and the operating life of the entire system, reducing the contaminant ingestion from the environment. The interaction between injected particles and the internal surfaces of the machine is responsible for different phenomena like deposition, erosion, and corrosion. Fouling is caused by the adherence of solid particles transported by the air, which are present in the environment [1, 2], moreover it can decrease the efficiency up to 3 % [3]. On the other hand, erosion is due to the impact between contaminants and internal surfaces, especially in the turbine stages [4]. The injection of water droplets causes corrosion and could significantly influence the gas turbine operation [5]. Different types of filtration systems, such as mechanical, inertial,

and electrostatic, are used to reduce the amount of contaminants entering the gas turbine. An ideal filter should have zero pressure losses and maximum filtration efficiency for all the inflow particle diameters and velocities. The combination of filtration mechanisms used for a specific application is selected according to gas turbine inlet velocity, main types of contaminants in terms of particle diameters and material, allowed pressure losses, maintenance time interval, and environmental conditions. To obtain a high filter efficiency for all the typical particle sizes present at the inlet of a gas turbine, a combination of filtration mechanisms is usually employed [6]. For instance, in [5] a filtering system based on a pre-filter and a high-efficiency filter is reported. This configuration is selected to allow an overall high filtration efficiency for a wide range of particle diameters. Inertial-diffusive separation systems can separate particles with big diameters, or in a better way, particles with higher Stokes numbers. Typically these devices are based on the Coanda effect. Smaller contaminants, tend to follow the streamline reducing the possibility of separating particles using the inertial effects, therefore other kinds of mechanisms i.e., mechanical separation and electrostatic precipitation are used to collect them. Electrostatic precipitators are used to collect micro-sized particles and to promote particle agglomeration. In recent years this separation mechanism has provided promising results for gas turbine applications as reported in [7]. The filtration mechanism is based on the possibility of separating the solid particles from the airflow through the effect of the electrostatic force. The electrostatic force generated by the electric field within the filtration system is useful for pushing particles onto the collector surface. The traditional electrostatic filters are pre-charged before the installation and therefore the effects of the electrostatic force vanish during the operating life of the filter.

The work aims to introduce a new electro-dynamic filtration system obtained by coupling an inertial element with a DC electric field that separates the particles with lower diameters due to the effect of the electrostatic force. In the innovative configuration, the electrostatic force does not change in time, as in the traditional electrostatic filter, due to the continuous application of the electrical potential. In the first part of the work, a numerical campaign is performed to assess the best geometry for the filtration system. To do that, an in-house electrostatic solver developed in OpenFOAM was used. In the second part, the best geometry is experimentally tested to validate the numerical results and assess the real filtration performance as the contaminants and exposure time vary. At the end of the work, a possible embedding of the developed concept in a real-scale application is evaluated.

2. Numerical approach and results

The traditional OpenFOAM release doesn't allow to take into account the electrostatic force on the discrete phase. Therefore, a new Lagrangian solver needs to be implemented. In the developed Lagrangian solver, the calculation of the electric field, E, and the electric potential, V has been introduced for the continuous phase. Moreover, the calculation of the electrostatic force acting on the discrete phase is introduced. The complete description of the numerical implementation and the validation of the solver against literature experimental data is reported in [8].

Figure 1 shows the general numerical domain used inside the work, in which the upper and the lowest surfaces are considered symmetry boundaries to reduce the computational burden required by the simulation. At the inlet of the domain a velocity inlet boundary condition of $1\,\mathrm{m\,s^{-1}}$ is imposed, this value is selected in order to approximate the typical airflow velocity at the inlet of a gas turbine filter house. The outlet, instead, a relative static pressure outlet boundary condition is set equal to $0\,\mathrm{Pa}$. Moreover, the voltage applied to the wire is adjusted for each geometry of the filter device to avoid the breakdown phenomena that occur when the electric field exceeds the threshold limits of $3\,\mathrm{MV\,m^{-1}}$ for the dry air.

The diameter distribution reported in Tab. 1 is employed in the current study. The selected

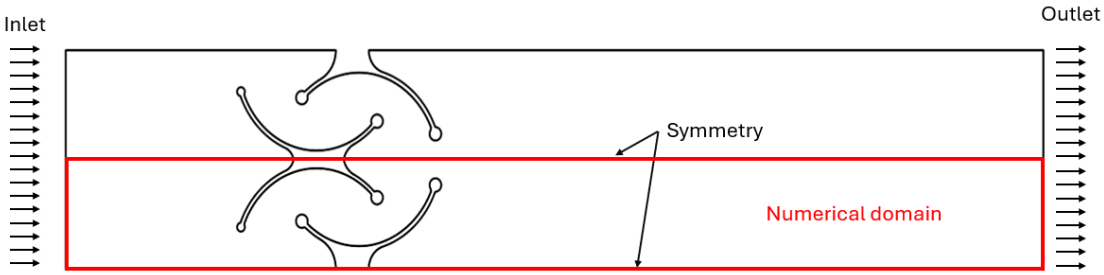

Figure 1: Numerical domain scheme.

Table 1: Details about the particle distribution used in the numerical simulations

	Value
Particle density $[kg/m^3]$	2700
Particle per second $[\#/s]$	403.19×10^3
Type of distribution	Normal
Mean diameter $[\mu m]$	1
Variance $[\mu m]$	0.5
Max Diameter $[\mu m]$	3
Min Diameter $[\mu m]$	0.5

distribution is representative of the particle size usually present at the inlet of a gas turbine [6]. A particle concentration of $1\,\mathrm{mg\,m^{-3}}$ is selected as a reasonable operative point of the ESP. The resulting particle mass flow rate is $\dot{C_m} = 0.57\,\mathrm{\mu g\,s^{-1}}$, with an volumetric air flow rate of $0.57 \times 10^{-3}\,\mathrm{m^3\,s^{-1}}$. Considering a mean diameter of the normal distribution equal to 1 µm, each particle has a mass of $1.41 \times 10^{-15}\,\mathrm{kg}$. OpenFoam requires as input for a lagrangian calculation the number of particles per second, which results equal to $N_p = \dot{C_m}/m_p = 0.57 \times 10^{-9}/1.41 \times 10^{-15} = 403.19 \times 10^3$ and the restitution coefficient of the boundary surfaces. Due to the effects of the electrostatic force, the total amount of particles that remain stuck on the grounded surfaces will be higher than the amount of the rebounded ones, for this reason, the stick condition is applied to these parts of the filtration system. For all the other surfaces an elastic rebound of the particles is set (restitution coefficients are set to one). The work does not consider particle agglomeration due to the high computational demand required for a four-way coupling simulation. Therefore a lagrangian two-way coupling approach is used.

The author aims to use CFD simulations to have a fast evaluation of the performance in terms of capture efficiency and pressure losses of an ESP. For this reason, a systematic evaluation of the ESP geometry is performed to assess the best geometry that minimizes the pressure losses, maximizes the capture efficiency, and ensures a safety margin for electrical breakdown. The parameters that are changed inside the optimization loop are the voltage applied to the wires, the number of the wires, the distance between the filter elements, and their shapes. The best-obtained geometry is reported in Fig. 2 in which the red dots represent the positions of the wires where the electrical potential is applied, while in blue are reported the grounded surfaces and in grey the insulated ones.

The flow path inside the system is reported in Fig. 3 in which a velocity contour is superimposed to a streamline plot. From this, it is possible to notice how the geometry promotes the recirculation of the flow inside the system, which allows the particles to agglomerate. The particle agglomeration is not considered in the simulation but it reasonably increases the filtration system's inertial effects, therefore increasing the device's overall efficiency. The

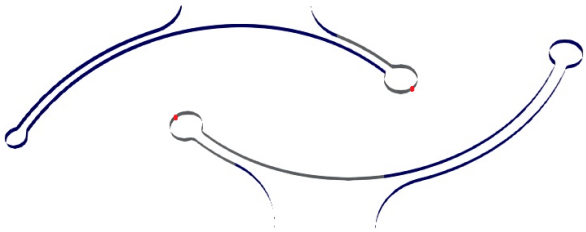

Figure 2: Filter elements geometry: grounded surfaces (blue), wires (red) and insulated surfaces (grey).

capture efficiency varies approximatively linearly with the electric potential applied to the wires. Therefore the electric potential is selected to avoid the breakdown phenomena, for the considered geometry an electric potential of 45 kV is applied to the wire. The resulting capture efficiency is close to 98 % with a pressure drop equal to 50 Pa.

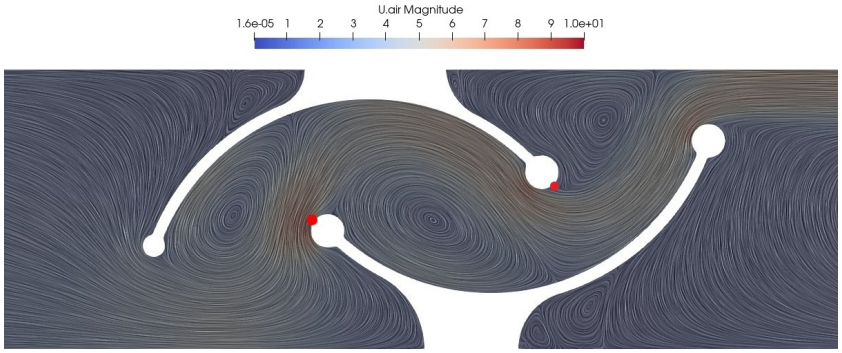

Figure 3: Velocity contour and streamline plot.

3. Experimental Campaign

The performance of the electro-dynamic filtration system are here evaluated in a lab-scale test campaign against different contamination scenarios.

3.1. Test Rig

The test rig consists of a ventilation duct with a standard side of 600 mm, located at the Mechanical Engineering Laboratories of the University of Ferrara. The airflow is provided by an 11 kW centrifugal fan located at the outlet to simulate a real-operating condition of the filter device. A sketch of the test bench with the main components and dimensions is reported in Fig. 4. Four main sections can be identified:

a) Inlet section: two HEPA media filters prevent the ingestion of unwanted pollutants from the outside air and a HVAC system controls the air conditions, i.e., temperature and humidity.

b) Contamination section: calibrated amounts of contaminants are injected in the test rig by means of a particle feeder. A metal sheet diaphragm coupled with a fine grid is installed to uniform the airflow velocity and the contaminants distribution throughout the duct section.

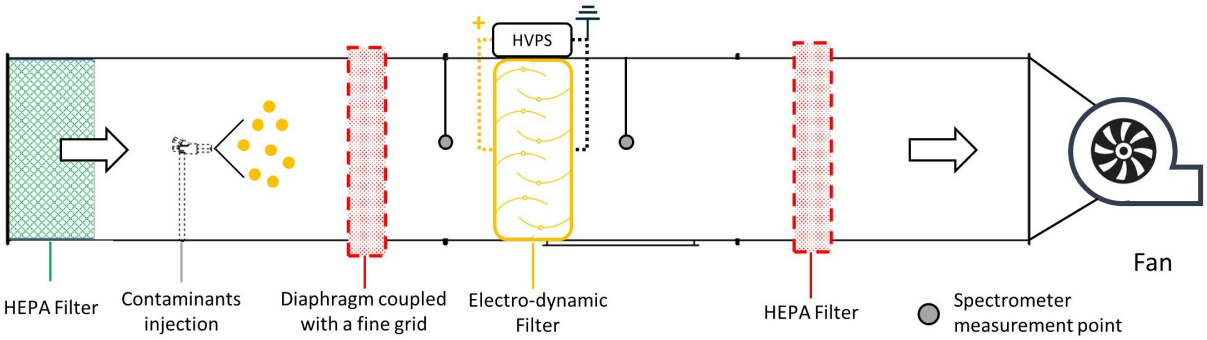

Figure 4: Test bench layout.

The shapes and characteristic dimensions for the diaphragm and the grid were optimized during preliminary CFD simulations of the flow field inside the duct.

c) Test section: the filter's performance is calculated by measuring the particles concentration upstream and downstream of the filter by means of an optical spectrometer. The measuring sections are located at 0.5 hydraulic diameters (equal to 150 mm) far from the filter inlet and outlet respectively. On purpose iso-kinetic probes are employed to achieve the isokinetic sampling of the spectrometer and to collect the particles in a parallel path [9]. A K-type thermocouple and an absolute pressure transducer (range of 0-2 bar) are placed at 1 hydraulic diameter before the filter to monitor air temperature and static pressure.

d) Outlet section: The residual contaminants are removed from the flow with an HEPA filter placed before the fan and the exhaust air is then conveyed outside.

The optimized filter shape obtained through numerical simulations (see Fig. 2) is considered for the present experimental campaign. The filter section consists of multiples of the filter module (Sec. 2) repeated in a row to cover the entire duct width, resulting in 12 filter modules for the actual test rig. A Spellman MXR30 DC high-voltage power supply (HVPS) is employed to generate an electric field able to influence the path of smaller particles and thus promoting their agglomeration. The output voltage of the HVPS is adjustable from 0 up to 30 kV. All the positive wires are connected to a conductive common rod. Applying a voltage difference between the electrodes and taking into account the effect of geometry, the resulting electric field E is calculated with Eq. 1, as reported by Bever *et al.* [10].

$$E = \frac{2U}{d} \tag{1}$$

Where U is the imposed potential difference, and d is the distance between the electrodes, which is set to 18 mm in the current analysis. The above equation is valid only for $d >> 2r$, where r is the wire radius. The particle feeder SAG 410 ultralow flow manufactured by TOPAS GMBH is employed to guarantee constant air contamination during tests. The powder is charged on a rotating ring through a worm screw and the it is carried at constant speed from the charging site to the ingestion dispersing nozzle that deagglomerates and disperses the powder. The rotation speed of the dosing ring can be set freely, changing the mass flow rate of the injected powder. More details regarding the calibration process of the instrument are reported in [9]. The TSI Optical Particle Sizer 3330 spectrometer is employed to measure the particle concentration upstream and downstream of the filter. All signals from the sensors are managed by an NI DAQ hardware system through an in-house software developed in LabVIEW environment.

3.2. Contaminants

Two types of contaminant are considered in this work: Arizona Road Dust (ARD) and Carbon Black (CB), representative of the contamination coming from natural sources (i.e., soil) and anthropogenic sources (i.e., residual of combustion processes) respectively. ARD is a natural-based powder consisting mainly of about 70 wt.% silica and 14 wt.% aluminum oxide and other minor iron, sodium, calcium, and magnesium oxides [11], while the CB is a paracrystalline carbon produced by the incomplete combustion of hydrocarbon and heavy petroleum products having characteristics very similar to the soot [12]. Two grades of ARD have been tested: (i) Nominal (0–3) μm (ARD N), and ISO 12103—3 Medium (ARD M). All of the soil samples are characterized by a density of 2717 kg/m^3. The diameter distributions of the tested powders are reported in Fig. 5.

3.3. Experimental Procedure

The instrumentation and the acquisition system are turned on for thirty minutes before carrying out the measurements to ensure the stability of the signals. In this experimental campaign the airflow speed in the duct is 1 m/s and the potential difference between the electrodes is set to 10 kV, resulting in an electric field equal to 1.11 kV/mm. According to the literature, the air breakdown occurs for an electric field of 3 kV/mm [13]. Preliminary tests were carried out to prove the device's safety for the selected electric field range and no breakdown condition was experienced. Contaminant powders are baked for 24 hours before the test to reduce their water content. During test, the contaminants concentration upstream and downstream of the filter section is acquired for one minute and the average value is registered. To evaluate the filtration performance of the device, three test methodologies are defined as follows:

(A) *Standard Capture Efficiency*: the filter is tested under real-operating conditions with the contaminants described in Sec. 3.2. A preliminary literature review (Sec. 1) suggests that a contaminant concentration range of (50 – 150) μg m^{-3} can be representative of industrial or desert areas in the absence of extraordinary atmospheric events (dust storms, volcanic eruptions, etc.). The detection of the over time behavior of the system is performed by measuring particle concentration at the filter inlet and the outlet section every 15 min, for a total duration of 10 h. Besides, the influence of relative humidity is investigated carrying out tests in dry (20 %RH) and wet conditions (80 %RH).

(B) *Maximum Load*: The maximum allowable dust load (on the ground electrode) will be defined by looking for drops in the capture efficiency. For this purpose, accelerated contamination tests able to reproduce longer exposure time (months) in lab-scaled test campaigns are arranged. Preliminary tests reported that dust concentrations between 100 μg m^{-3} and 1000 μg m^{-3} in wet conditions (80 %RH) for tens of hours of operation are necessary to detect drops in the device's performance. Since a low relative humidity delays the particle

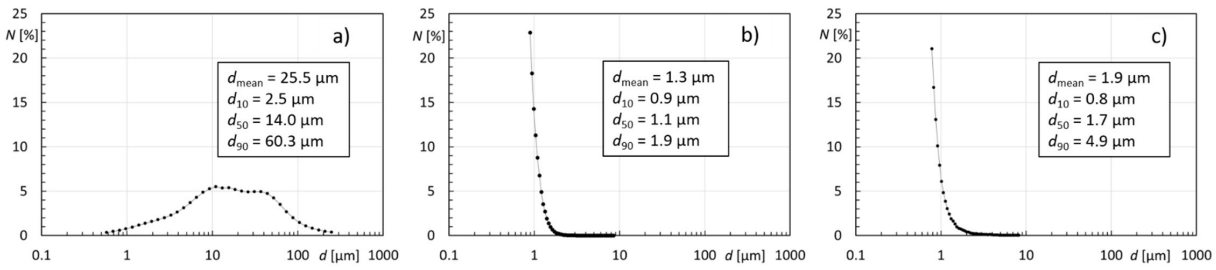

Figure 5: Distributions of contaminants diameter - a) ARD Medium; b) ARD Nominal; c) Carbon Black.

adhesion process on walls [14], and therefore the time to reach the maximum dust load, dry tests will not be considered in this methodology.

(C) *Maximum Concentration*: Test increasing the contaminant concentration allows to define the maximum acceptable concentration by the filter before reducing the capture performance. A reference value is obtained by measuring the capture efficiency for one hour with contaminant concentrations equal to those of Methodology A (50 – 150) μg m^{-3}. Then, tests at higher contaminant concentrations are carried out. The maximum concentration value is defined when a performance drop of 50 % of the average capture efficiency (results of Methodology A) is experienced. Here, the powder concentrations aim to be representative of severe weather events, e.g. dust storms, volcanic ash, and bushfires. In this way, concentrations in the order of 10^3 μg m^{-3} are considered [15, 16, 17]. Test were performed at 50 %RH with the coarser soil particles (ARD M) and soot (CB) as contaminants.

The complete description of the experimental approach and strategy is reported in [18].

4. Experimental results

The filtering performance are evaluated by measuring the particle mass distribution and then computing the capture efficiency as follows:

$$\eta = \frac{C_i - C_o}{C_i} \cdot 100 \tag{2}$$

where C is the contaminant mass concentration $[\mu g \cdot m^{-3}]$, and the subscripts i and o refer to the filter inlet and the outlet section respectively. The results here reported are normalized with the highest capture efficiency number-based experienced during the test campaigns, i.e., ARD M in methodology B.

4.1. Methodology A - Standard Capture Efficiency

The dimensionless overtime capture efficiency η in real-life contamination scenarios are reported in Fig. 6. The overall performance can be summarized as follows. According to the ISO 16890 standard, the filtration system belongs to the filter class ISO ePM2.5 60 %. In light of this, the filter in its actual configuration can find application in the pre-filtration stages of the intake or in the auxiliary ventilation system of the enclosure. The maximum capture efficiency experienced during the test campaigns, i.e., ARD M in methodology B, is considered to reduce the results in dimensionless form. The coarser soil powder (ARD M) experiences the highest capture efficiency in both dry and wet conditions due to the greater effectiveness of the inertial effect on bigger particles. For finer soil particles (ARD N) the capture efficiency reduces by factor 0.6 and 0.7 in wet and dry conditions respectively compared to the performance with ARD M. On the other hand, with soot (CB) even lower efficiencies are obtained: the performance with ARD M is reduced by a factor of 0.35 in wet condition and 0.25 in dry condition. Even if CB and ARD N are characterized by a similar diameter distribution, the resulting capture efficiency demonstrates that the soot particles are more difficult to remove from the airflow through the imposed electrostatic field.

4.2. Methodology B - Maximum Load

The dimensionless overtime capture efficiency for the long-exposure test with ARD M and CB is reported in Fig. 7. The scaling process on particle concentration for the time interval Δt is based on the calculation of the Equivalent Dose D by Clarkson *et al.* [19].

$$D = C \cdot \Delta t \tag{3}$$

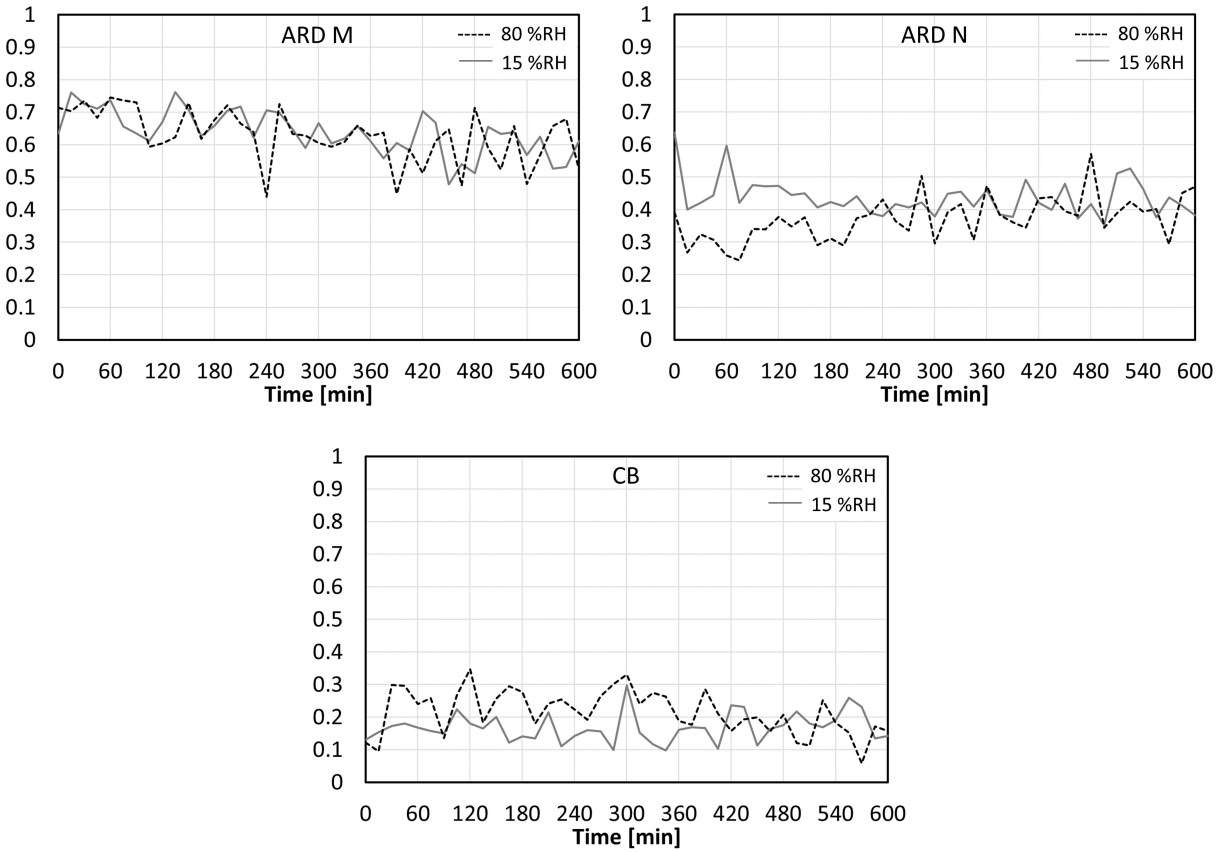

Figure 6: Results Methodology A - Dimensionless capture efficiency overtime.

and the total injected mass M is obtained:

$$M = D \cdot \frac{\dot{m}_a}{\rho_a} \tag{4}$$

where $\dot{m}_a$ is the air mass-flow rate and ρ_a is the air density. For soil particles (ARD M), the total exposure time is 2580 min (43 h) with a total amount of injected mass of 205 g. remarkable fluctuations in filtering performance are detected after 1500 min (25 h) of testing and 33 g of ingested sand. Both the average capture efficiency and the potential difference are reduced due to the presence of a deposited layer of particles. The correspondent soil dust load limit on the ground plate is found equal to 36 g/m^2. A similar trend is found for soot particles (CB) by a shorter exposure time (Fig. 7b). Drops in the average capture efficiency and potential difference among the electrodes take place after 330 min (5.5 h) of exposure time and thus 1.6 g of injected powder. The resulting dust load limit for soot is found for 0.4 g/m^2. Estimation of the exposure duration without restoring: with the hypothesis of a particle concentration of 5 μg/m^3, the maximum exposure time is 5000 h (208 days) for soil particles and 220 h (9 days) for soot.

4.3. Methodology C - Maximum Concentration

To assess the maximum dust load allowable at the filter inlet, the particle concentration (soil and soot) was increased, and the capture efficiency was monitored simultaneously. Concentrations typical of Methodology A (50-150) μg m^{-3} are considered for one hour to obtain the reference efficiency, which is found equal to 75 % and 22 % of the reference value, for soil and soot particles respectively. Then, the threshold for determining the maximum concentration is

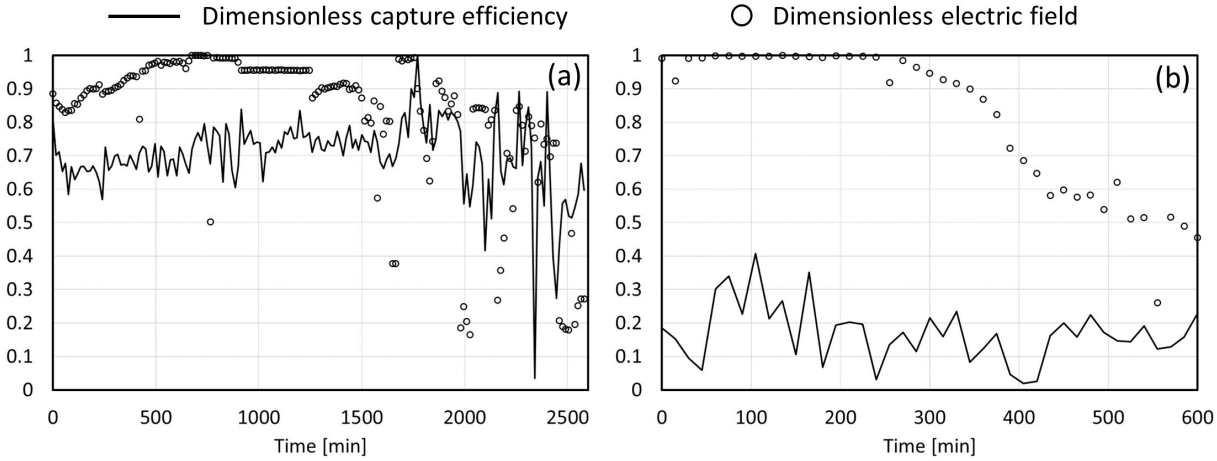

Figure 7: Results Methodology B - Max Load: a) ARD M (soil); b) CB (soot).

obtained by observing a reduction of the performance up to 50 % of the average capture efficiency experienced. The final assessment shows the following performance:

- Soil (ARD M): maximum dust concentration at the inlet equals 12 mg/m^3;
- Soot (CB): maximum dust concentration at the inlet equals 0.5 mg/m^3.

5. Actual application analysis

The last part of the present analysis is devoted to analyzing the possibility of embedding the developed concept in an actual application. The effect of dimension will be investigated by embedding the module in an actual filter house that is commonly used in power plants. The dimensions of the intake geometry and the distance to filterless were accounted for in the investigation of the flow disturbance introduced by the original shape of the filterless elements. In the Fig. 8, the dimension of the considered filter house. In such a configuration, the filter house has 150 filterless modules with a frontal dimension of 600 mm x 600 mm. The filterless modules were installed in the straight section, equally distanced from the inlet to the convergent section. The filter house also reduces section area, which is helpful to connect the filtration system to the gas turbine unit.

Four detection sections were taken into account to evaluate the velocity distribution and account for the wake and disturbance phenomena introduced by the original shape of the module. This detection allows the definition of the flow uniformity after the module section. The distance from the module was defined according to the characteristics length of the module. The four detection sections were positioned at 150 mm, 300 mm, 600 mm, and 1200 mm, corresponding to L/4, L/2, L, and 2L, respectively. The length L is the module length, and it equals 600 mm.

The uniformity index was used to quantify the flow field uniformity. The uniformity index expresses how a defined scalar quantity is distributed along a surface or a line. When the scalar quantity is equally distributed, a value of ϕ equal to 1 is obtained. In the present analysis, the following formula was applied to calculate the uniformity index [20]:

$$\phi = 1 - \frac{\sum_{i=1}^{N} (\phi_i - \phi_{ave}) L_i}{2\phi_{ave} \sum_{i=1}^{N} L_i} \tag{5}$$

where ϕ_{ave} is the average value of the variable (velocity), and ϕ_i is the local value of the variable associated with the length L_i (local grid spacing).

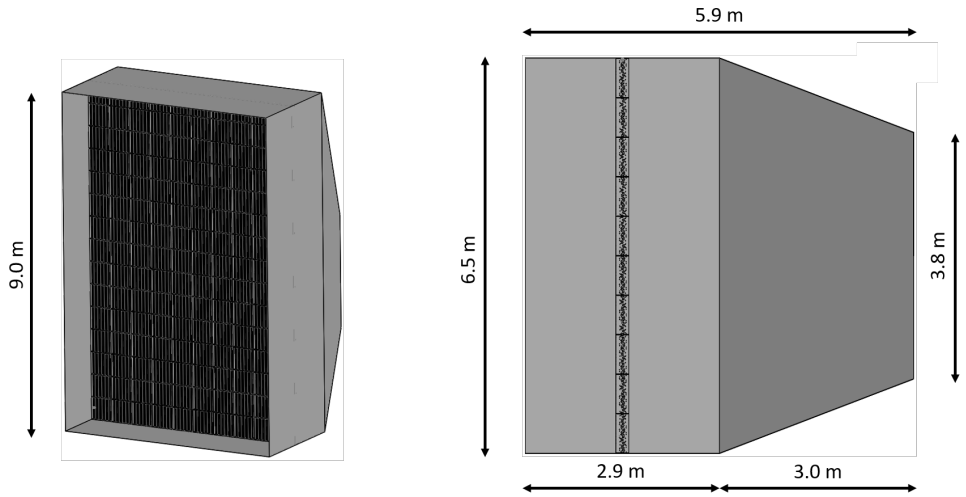

Figure 8: Filter house dimension

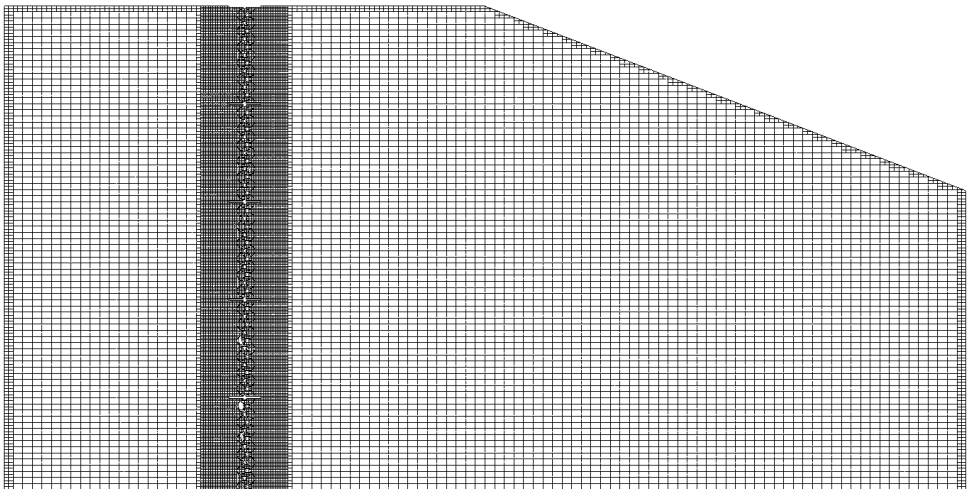

Figure 9: Computational mesh realized with the cut-cell approach. The inlet section is on the left hand side.

The analysis of the full-scale filter house equipped with the filterless device involved an air velocity of 1 m/s, corresponding to the designed value. A computational model was developed for the entire filter house. A cut-cell meshing strategy was adopted, and the computational mesh comprised about 10 M elements. A specific refinement was adopted in correspondence with the filter device to detect the flow structure within the filter elements. A footprint view of the computational mesh adopted is reported in Fig. 9 where the mesh element distribution and the local refinement can be appreciated.

Adiabatic wall conditions were imposed at the boundaries, and a uniform velocity inlet (1 m/s) and a relative static pressure of 0 Pa were imposed at the inlet and outlet, respectively. At the inlet, a low turbulent kinetic energy was adopted to reproduce the actual condition of the filter house. For the closure of the turbulent problem, a Lam-Bremhorst low-Reynolds-number $\kappa - \varepsilon$ model was adopted. The results of the analysis are reported in the Fig. 10. The figure shows velocity contour plots for the top and side views of the filter house. In addition, the velocity profiles are reported according to the four detection segments described above. In the

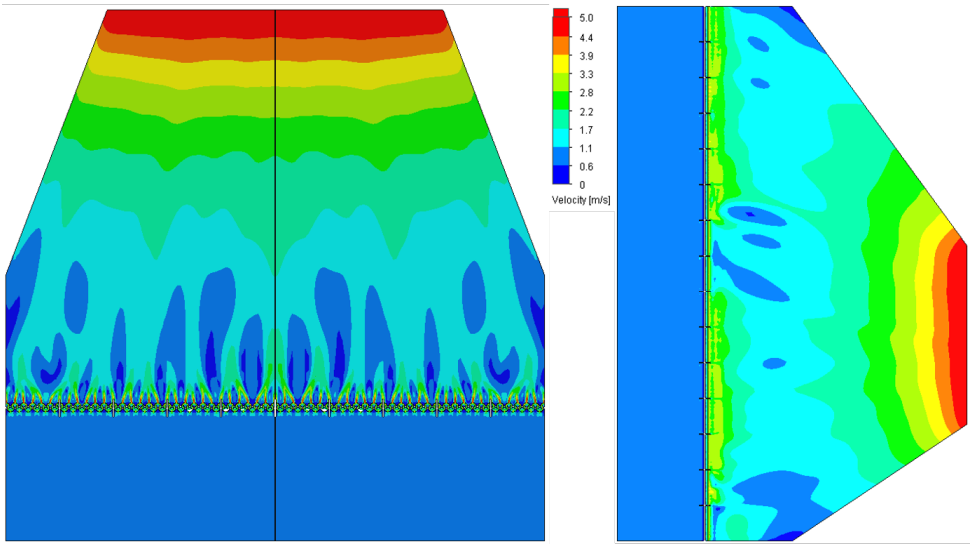

Figure 10: Velocity flow field from top and side view of the filter house for 1 m/s.

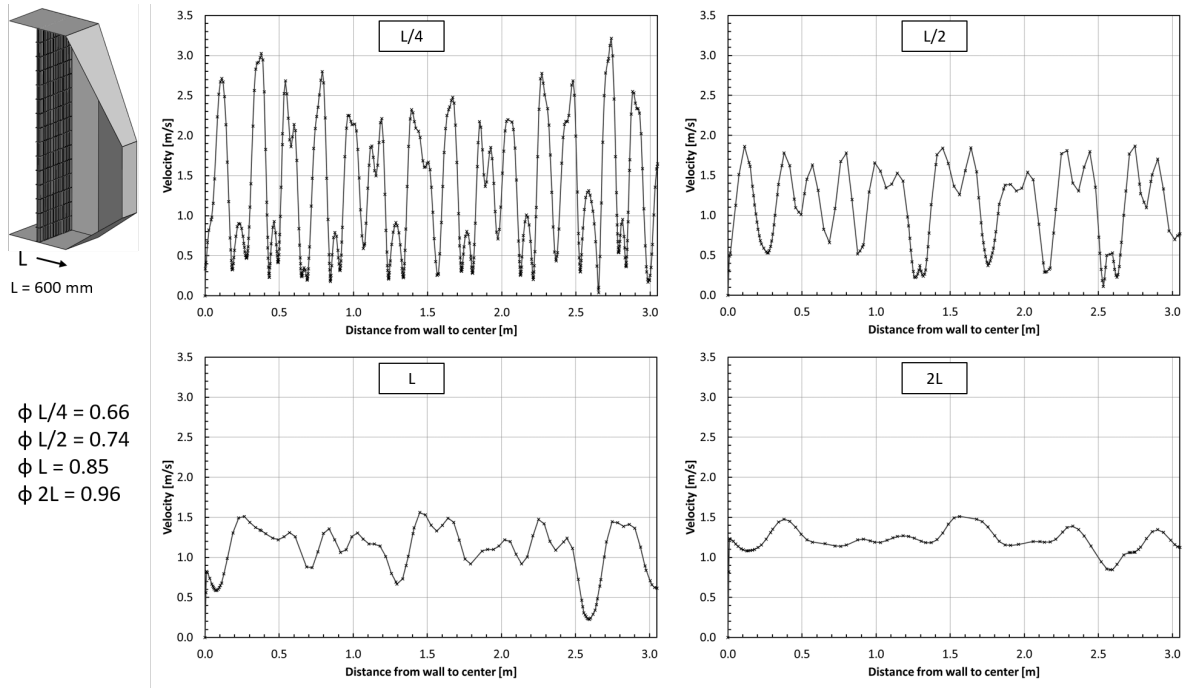

Figure 11: Velocity profile for the four detection segments (L/4, L/2, L, and 2L) for 1 m/s. The uniformity index values are also reported.

Fig. 11, the values of the uniformity index are also reported. It can be seen that the wake of the module is almost negligible after 1200 mm (2L).

6. Conclusions

In this analysis, a new concept for managing the filtration mechanisms of a gas turbine has been proposed. The basic idea is to exploit the capability of the electric field to interact with the micro-sized solid particles. Starting from the conceptualization, a specific numerical model

has been carried out to design and optimize the shape and the system. A set of experimental tests on a 1:1 filter module has been managed to prove the capability of the system to separate micro-sized particles from the airflow stream. Experimental tests have demonstrated that the basic concept can separate natural-based contaminants (soil) and artificial-based particles (soot). Finally, a 1:1 filter house has been analyzed using computational analysis to discover the flow uniformity after the filtering module. The preliminary results in terms of efficiency and the reduced pressure drop of the system show a great potential application to the land-based gas turbine unit.

References

[1] Suman A, Morini M, Aldi N, Casari N, Pinelli M and Spina P R 2017 *Journal of Turbomachinery* **139** 041005
[2] Suman A, Casari N, Fabbri E, di Mare L, Montomoli F and Pinelli M 2019 *Progress in Energy and Combustion Science* **74** 103–151
[3] Igie U, Pilidis P, Fouflias D, Ramsden K and Laskaridis P 2014 *Journal of turbomachinery* **136** 101001
[4] Casari N, Pinelli M, Suman A, di Mare L and Montomoli F 2018 *Journal of Turbomachinery* **140** 061001
[5] Wilcox M 2011 *Mechanical Engineering* **133** 48 – 49
[6] Wilcox M, Baldwin R, Garcia-Hernandez A and Brun K 2010 *Guideline for gas turbine inlet air filtration systems - Gas Machinery Research Council, Dallas, TX*
[7] He Z, Dass E M and Karthik G 2017 *Journal of Aerosol Science* **108** 14 – 28
[8] Pinelli M, Piovan M, Suman A, Zanini N, Rossin S and Minotti S 2024 *Proceedings of the ASME Turbo Expo, Article under pubblication* Paper number GT2024–128641
[9] Suman A, Zanini N, Vulpio A and Pinelli M 2024 *Experimental Thermal and Fluid Science* **151** 111074
[10] Bever R S, Ruitberg A P, Kellenbenz C W and Irish S M 2006 High voltage power supply design guide for space Tech. rep. URL `https://ntrs.nasa.gov/citations/20070013972`
[11] ISO-12103-1 2016 *Road Vehicles—Test Contaminants for Filter Evaluation—Part 1: Arizona Test Dust*
[12] Omidvarborna H, Kumar A and Kim D S 2015 *Renewable and Sustainable Energy Reviews* **48** 635 – 647
[13] Paschen F 1889 *Annalen der Physik* **273** 69 – 96
[14] Suman A, Vulpio A, Casari N and Pinelli M 2021 *Powder Technology* **394** 597 – 607
[15] Hoffmann C, Funk R, Sommer M and Li Y 2008 *Atmospheric Environment* **42** 8422 – 8431
[16] Scollo S, Boselli A, Coltelli M, Leto G, Pisani G, Prestifilippo M, Spinelli N and Wang X 2015 *Geophysical Research Letters* **42** 2634 – 2641
[17] Karthikeyan S, Balasubramanian R and Iouri K 2006 *Journal of Toxicology and Environmental Health - Part A: Current Issues* **69** 1895 – 1908
[18] Zanini N, Suman A, Piovan M, Pinelli M, Rossin S and Minotti S 2024 *Proceedings of the ASME Turbo Expo, Article under pubblication* Paper number GT2024–128568
[19] Clarkson R J, Majewicz E J and Mack P 2016 *Proceedings of the Institution of Mechanical Engineers, Part G: Journal of Aerospace Engineering* **230** 2274 – 2291
[20] Om Ariara Guhan C, Arthanareeswaran G, Varadarajan K and Krishnan S 2016 *Journal of Computational Design and Engineering* **3** 198 – 214